




# Parametric Optimisation for Extraction of the Nanosized Cathodic Material from the Lithium-Ion Battery Waste Material

Vivek Kumar Sharma <sup>1</sup>, Gaurav Sharma <sup>2</sup>, Varun Pratap Singh <sup>1,3</sup>, Siddharth Jain <sup>1,\*</sup>

<sup>1</sup> Mechanical Engineering Department, School of Advanced Engineering, UPES, Dehradun 248007, India, vivek.113654@stu.upes.ac.in (V.K.S.); varunpratap.singh@ddn.upes.ac.in (V.P.S.); siddharth.jain@ddn.upes.ac.in (S.J.);

<sup>2</sup> International Research Centre of Nanotechnology for Himalayan Sustainability (IRCNHS), Shoolini University, Solan 173229, India; gaurav.541@shooliniuniversity.com;

<sup>3</sup> Solar Thermal Energy Research Group, Mechanical and Mechatronics Engineering Department, Stellenbosch University, South Africa; vpsingh@sun.ac.za;

\* Correspondence: arthjain2001@gmail.com;

Received: 10.06.2025; Accepted: 19.07.2025; Published: 25.11.2025

**Abstract:** This research presents an advanced, integrative framework for the recovery and nanoscale refinement of LiCoO<sub>2</sub> cathodic material derived from spent lithium-ion batteries. The principal innovation of this study lies in the strategic, sequential implementation of direct recycling, pyrometallurgical calcination, and hydrometallurgical leaching, followed by a statistically optimized ball-milling process. This hybrid methodology departs from traditional single-stream recycling approaches by simultaneously enhancing material recovery efficiency and preserving structural integrity. Employing Response Surface Methodology (RSM) with a Box-Behnken Design across 27 experimental trials, the study systematically optimized four key ball milling parameters—milling duration, ball diameter, ball-to-material weight ratio, and rotational speed—for their influence on particle size before and after the leaching phase. Regression modeling and analysis of variance (ANOVA) indicated excellent model fidelity, with rotational speed and its interaction effects emerging as the most statistically significant contributors post-leaching. Under optimized milling conditions (60 minutes, 5 mm ball diameter, 30:1 ratio, and 650 rpm), particle sizes below 120 nm were consistently achieved, with predictive error margins maintained at < 5%. The outcomes of this investigation establish a novel, scalable, and environmentally viable process for nanoscale cathode recovery, making a substantive contribution to advancing sustainable resource management and circular economy initiatives in the energy storage domain.

**Keywords:** lithium-ion battery recycling; LiCoO<sub>2</sub>; nanoscale cathodic recovery; ball milling optimization; response surface methodology (RSM); sequential recycling; hybrid processing; pyrometallurgy; hydrometallurgy; sustainable circular economy.

© 2025 by the authors. This article is an open-access article distributed under the terms and conditions of the Creative Commons Attribution (CC BY) license (<https://creativecommons.org/licenses/by/4.0/>), which permits unrestricted use, distribution, and reproduction in any medium, provided the original work is properly cited. The authors retain copyright of their work, and no permission is required from the authors or the publisher to reuse or distribute this article, as long as proper attribution is given to the original source.

## 1. Introduction

The rapid adoption of lithium-ion batteries in consumer electronics, electric vehicles, and renewable energy storage has led to a significant increase in global battery waste [1, 2]. The disposal of spent lithium batteries poses significant environmental and economic challenges due to their toxic and hazardous components, including heavy metals such as cobalt, nickel, and

lithium [2-4]. A number of nations have implemented regulations and frameworks for the management of LiB waste, emphasizing effective recycling and resource recovery [5, 6]. Although advanced countries such as the EU, the United States, and China have established rigorous policies, India is still in the early stages of building a robust recycling infrastructure [7-9]. The recent regulations from the Indian government, such as the Battery Waste Management Rules 2022, highlight the importance of Extended Producer Responsibility (EPR) and encourage the development of sustainable recycling technologies [10, 11].

The recycling of spent lithium batteries is crucial for several reasons, including conserving vital materials, reducing environmental pollution, and reducing reliance on the extraction of raw materials [12], [13], [14]. The rising demand for lithium-ion batteries necessitates the recovery of valuable metals such as lithium, cobalt, and nickel from waste batteries, which is essential for the sustainable advancement of the battery sector [15-17]. Furthermore, the improper disposal of lithium batteries poses significant environmental risks, including the potential for groundwater contamination and fire hazards from flammable electrolytes [17]. A variety of recycling technologies have been investigated for the recovery of cathodic materials from spent lithium batteries, which can be broadly classified into DR, PT, and HT. DR focuses on preserving the integrity of cathodic materials through minimal processing, while pyrometallurgical methods utilize high-temperature smelting to recover metal alloys [18], [19], [20]. Hydrometallurgical techniques employ chemical leaching to selectively extract metal ions, thereby enhancing material purity and reducing energy consumption [21], [22]. Recent investigations have focused on refining these methods to improve efficiency, reduce reagent use, and the economic feasibility of LiB recycling [24].

Although there has been notable progress in LIBS recycling, various deficiencies remain in the existing literature. Challenges encompass the significant energy demands associated with pyrometallurgical processes, the production of secondary waste streams in hydrometallurgy, and the deterioration of cathode material structure in DR. Furthermore, the constrained scalability of existing recycling techniques, along with irregular waste collection systems, obstructs the broad implementation of sustainable recycling practices.

This experimental study systematically evaluates the effectiveness of various process parameters during cathodic material size reduction using ball milling and optimizes the most effective process parameters for this reduction. The recycling techniques have been applied in sequence, DR, PT, and HT, for the recovery of cathodic materials from spent lithium batteries. This study enhances understanding of recovered materials, aiding the development of effective, scalable, and eco-friendly strategies for lithium-ion battery recycling.

## 2. Materials and Methods

### 2.1. Materials.

This experimental investigation utilizes Lithium-ion battery packs, namely the "18650 Hongali 2600 MAH Lithium-ion Cell EV Grade" as the primary components. The composition of these battery packs is  $\text{LiCoO}_2$ . Chemicals including  $\text{H}_2\text{SO}_4$  for Pretreatment process in DR, Crucibles for waste material calcination in PR, and hydrogen peroxide ( $\text{H}_2\text{O}_2$ ), citric acid, used for leaching in HR, are procured from SANMATI ENTERPRISES, Manufacturer and Dealers of Scientific Instruments, located at 341, 7 Civil Lines, Roorkee- 247 667 (Uttarakhand), India, and possess a minimum purity of 99.99% quality. These chemicals are commonly used in leaching and reduction procedures.

## 2.2. Experimental procedure.

### 2.2.1 Dismantling and direct recycling (DR).

The primary objective of this experimental study is to convert LIBS cathodic powdered material into nanoscale dimensions to demonstrate the experimental procedure, as shown in Figure 1. Initially, LIBS underwent DR, during which the batteries were dismantled and pretreated with  $H_2SO_4$ , followed by oven heating at  $100\text{ }^\circ\text{C}$  for 1 hour. During the dismantling process, all physical materials, including steel, plastics, aluminum, and copper components, are recovered for reuse in the manufacturing of lithium-ion batteries and other applications.

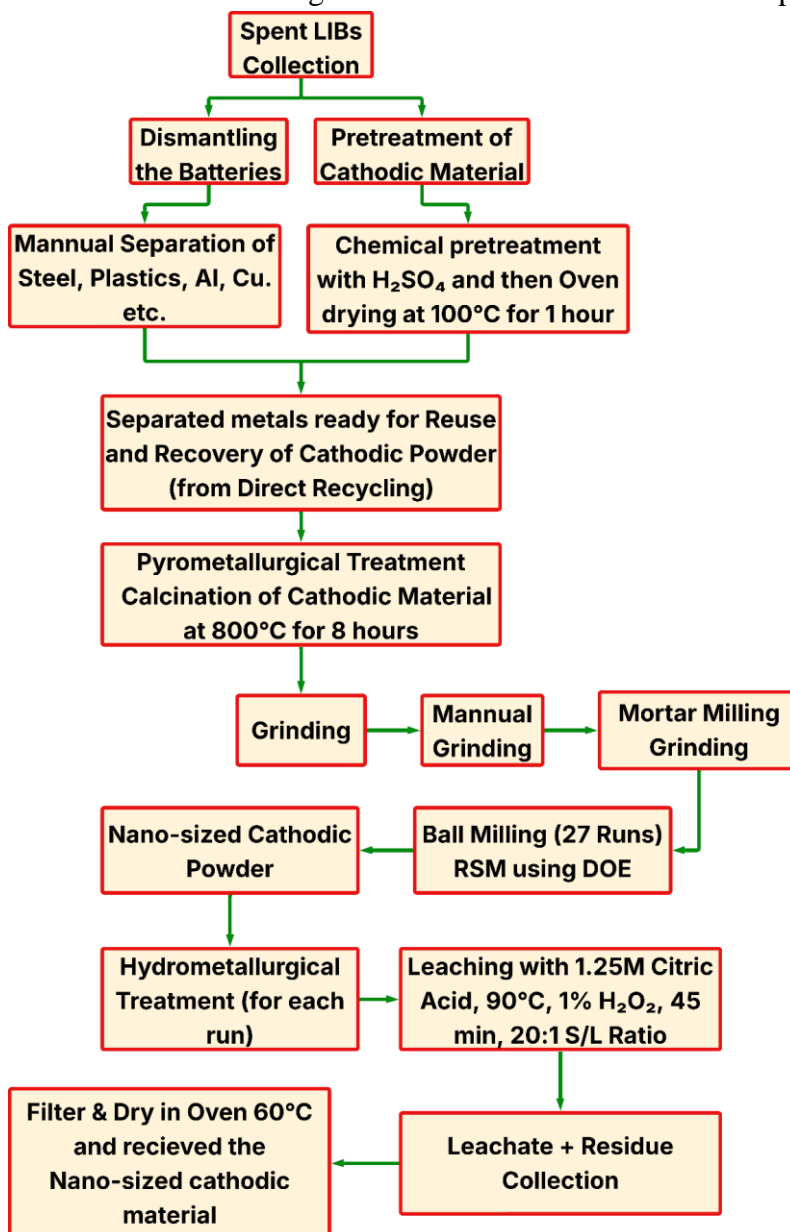


Figure 1. Experimental procedure.

### 2.2.2. Pyrometallurgical treatment (PT).

The pretreated cathodic material from DR was subjected to calcination at  $800\text{ }^\circ\text{C}$  for 8 hours. This thermal treatment helped eliminate  $CO_2$ . The resulting powder was ground in stages: manually in a mortar and pestle, then in a ball mill to reduce particle size to the micron scale.

### 2.2.3. Grinding and ball milling.

The cathodic material obtained from this treatment has undergone manual grinding to reduce its size. Subsequently, the material was ground using a mortar and pestle to achieve further size reduction. Following manual and mortar milling, the material has been reduced to the micron level. Ball milling has been conducted to reduce material size from the micron to the nanoscale, following the selection of an experimental design using Design of Experiments (DoE) with Response Surface Methodology (RSM).

### 2.2.4. Process parameter selection and DoE.

Through a comprehensive literature review, the factors influencing reduced response parameter sizes were identified. The variables chosen for the current experimental investigation include Time, Ball Sizes, Ball to Material ratio, and Speed of rotation. Table 1 presents the various factors examined along with their corresponding levels. The levels were allocated to each factor based on initial experimental findings [24-27].

**Table 1.** Process parameters with their levels [24-27].

S. No	Process Parameter	Unit	Level 1	Level 2	Level 3
1	Time	min	60	120	180
2	Ball diameter	mm	5	8	10
3	BW/MW ratio	–	10:1	20:1	30:1
4	Speed of rotation	rpm	250	625	1000

Every parameter is adjusted across three levels to facilitate an in-depth examination of its impact on the target response variable. This systematic method facilitates the creation of a second-order polynomial model in RSM, enabling the assessment of linear and interaction effects among the variables to enhance process performance.

The experimental design was developed in Design-Expert software, incorporating the selected process parameters and their respective levels within specified ranges, as detailed in Table 2.

**Table 2.** Experimental design.

Experimental run	Time	Ball-diameter	Ratio	RPM
1	120	10	20	250
2	120	5	10	625
3	60	8	10	625
4	120	8	20	625
5	120	10	10	625
6	120	8	20	625
7	180	8	10	625
8	120	8	10	250
9	60	5	20	625
10	180	5	20	625
11	120	5	30	625
12	120	5	20	250
13	120	8	10	1000
14	120	8	30	1000
15	120	5	20	1000
16	180	8	30	625
17	180	8	20	1000
18	180	10	20	625
19	60	10	20	625
20	120	8	30	250

Experimental run	Time	Ball-diameter	Ratio	RPM
21	120	8	20	625
22	60	8	20	1000
23	120	10	20	1000
24	60	8	20	250
25	180	8	20	250
26	60	8	30	625
27	120	10	30	625

The 27 experimental runs systematically adjust these parameters across various levels to examine their distinct and combined effects on the results. The design incorporates repeated conditions (e.g., runs 4, 6, and 21) to evaluate reproducibility and ensure statistical reliability. Ball milling was performed using this experimental design. After taking each and every experiment,

### 2.2.5. Hydrometallurgical treatment (HT).

Hydrometallurgical treatment has been performed for every individual experiment. In this treatment, the leaching process was conducted using the following parameters: Citric acid at a concentration of 1.25M, a temperature of 90°C, a 1% liquid solution of H<sub>2</sub>O<sub>2</sub> as the reducing agent, a running time of 45 minutes, and a S/L ratio of 20:1. The completed experiments are shown in Figures 2 and 3.

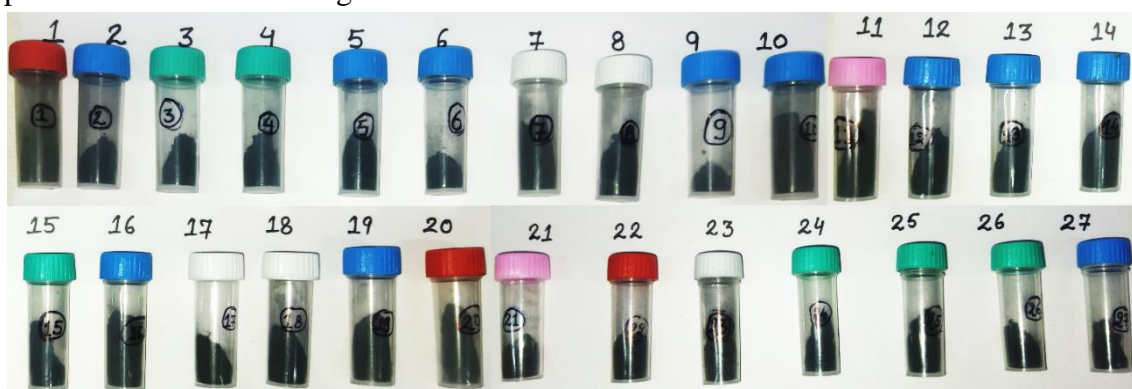


**Figure 2.** Photographic representation of cathodic material samples after ball milling but before leaching. The image shows the variation in texture and granularity across different runs, indicating the effect of milling parameters on initial particle reduction.

Each milled sample underwent hydrometallurgical leaching under standardized conditions. Figure 2 shows the appearance of the samples after ball milling, but before the leaching step. Variations in surface texture and density reflect differences in the milling parameters applied across runs.

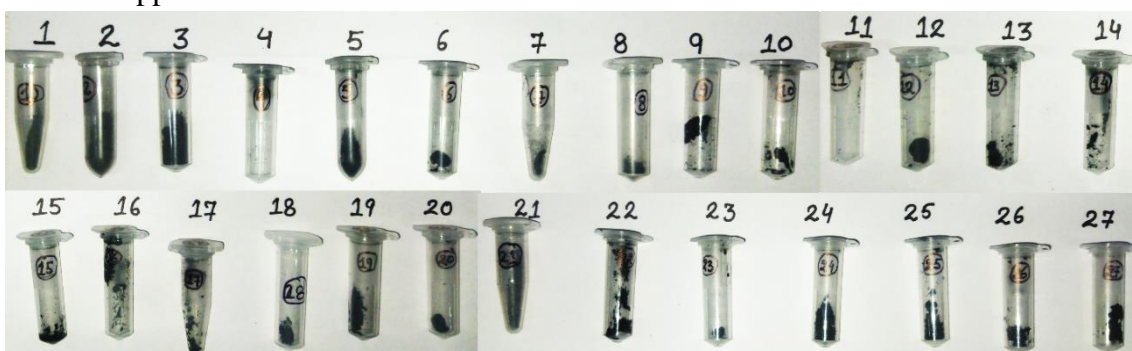


**Figure 3.** Visual comparison of post-leaching cathodic material from all 27 experimental runs. The increased homogeneity and fineness of the samples reflect successful leaching and particle-size refinement.

Figure 3 shows the same set of samples after undergoing leaching. The resulting material appears visually finer and more homogeneous, demonstrating the effectiveness of the leaching process in further reducing particle size. These images complement the quantitative particle-size data, providing visual validation of the material transformation through the sequential process.

### 2.3. Experimental design.

A review of the existing literature indicates that RSM is a cost-effective tool for modelling and optimization across various research endeavours. This technique has been applied in diverse scientific studies related to renewable energy, food engineering, and petrochemical engineering. The experimental design utilized in this study was the Box-Behnken Design. The four process variables were utilized as input parameters, with nanosized material (in nm) serving as the output response. The BBD matrix comprised 27 experimental runs [28].

### 2.4. Statistical analysis.

Experimental data underwent regression and graphical analysis. The nanosized material (in nm) was regarded as an output variable throughout the experimental design process. The experimental data were analysed using a second-order polynomial response surface regression equation [29]. The regression equation is presented below:

$$Y = \beta_0 + \sum_{i=1}^K \beta_i X_i + \sum_{j=1}^K \beta_j X_j^2 + \sum_{t=1}^{J-1} \sum_{l=2}^K \beta_{tl} X_t X_l + \varepsilon \quad (1)$$

In this equation, Y represents the response expressed in percentage terms, i and J denote the linear and quadratic coefficients,  $\beta$  signifies the regression coefficient, X indicates the process variable, and K reflects the number of factors that were examined.

### 2.5. Characterizations of experimental Run.

The objective of the present experimental study is to reduce the cathodic material size. For checking or verifying how much size has been reduced or how much size is obtained at each step and in each experimental run, it is necessary to check the particle size. Particle size was measured using a particle size analyzer (PSA). PSA is the characterization machine that exhibits all the aspects of testing particles. XRD and ICP-OES analyses have also been performed to assess the performance of the extracted cathodic material.

## 3. Results and Discussions

### 3.1. Effect of ball milling parameters before leaching.

Table 3 summarizes the particle size results before and after leaching for all 27 experiments. Notably, combinations of small ball size (5 mm), shorter milling time (60 min), high BW/MW ratio (30:1), and moderate RPM (650 rpm) yielded the best size reduction. Each entry corresponds to a unique experimental run, with essential parameters including milling time, ball diameter, ball-to-powder weight ratio, and milling speed (rpm) varying. The main aim is to investigate how these parameters affect the reduction of material size, which is

essential for effective leaching and recovery of valuable components from lithium-ion battery waste.

Table 3 also illustrates the relationship between milling conditions and particle size transformation, providing valuable insights for optimizing the process to produce nanosized materials that can be effectively reused in energy storage or catalytic applications.

**Table 3.** Experimental results on the cathodic material size basis.

STD	Run	Time (minutes)	Ball diameter (mm)	BW/MW ratio	RPM	Material size before leaching	Material size after leaching
22	1	120	10	20	250	131.8	112.9
13	2	120	5	10	625	250	120
17	3	60	8	10	625	209.4	180.55
27	4	120	8	20	625	250	190
14	5	120	10	10	625	92.09	150.66
26	6	120	8	20	625	217.7	180
18	7	180	8	10	625	170	120
5	8	120	8	10	250	300	114.1
1	9	60	5	20	625	166.7	82.68
2	10	180	5	20	625	90	172.5
15	11	120	5	30	625	150.9	127.7
21	12	120	5	20	250	155.9	151.56
7	13	120	8	10	1000	77.87	148.4
8	14	120	8	30	1000	220	37.84
23	15	120	5	20	1000	190.1	62.5
20	16	180	8	30	625	250	155.55
12	17	180	8	20	1000	68.6	142.3
4	18	180	10	20	625	85.57	98.88
3	19	60	10	20	625	93.19	170
6	20	120	8	30	250	135.6	160
25	21	120	8	20	625	210	189.8
11	22	60	8	20	1000	81.2	70
24	23	120	10	20	1000	77.58	99.66
9	24	60	8	20	250	141.2	171
10	25	180	8	20	250	158.1	145.68
19	26	60	8	30	625	125.6	120.56
16	27	120	10	30	625	248.2	120

3.2. ANOVA and model accuracy for pre-leaching.

ANOVA results (Table 4) indicate that ball diameter ( $p = 0.0183$ ) and rotation speed ( $p = 0.0101$ ) significantly influenced particle size reduction. Interactions such as BC (ball diameter  $\times$  BW/MW ratio) and CD (BW/MW ratio  $\times$  RPM) were also significant. Quadratic terms for time, ball diameter, and RPM confirm the presence of non-linear effects. The overall model is statistically robust, with a high F-value (8.87) and a low p-value (0.0003), confirming that the selected parameters jointly exert a significant influence on the response variable.

**Table 4.** F and P values for cathodic material reduction.

Source	Sum of squares	df	Mean square	F-value	p-value	
Model	1.051E+05	14	7504.43	8.87	0.0003	Significant
A-Time	2.07	1	2.07	0.0024	0.9614	
B-Ball Dia	6309.88	1	6309.88	7.45	0.0183	
C- BW/MW Ratio	79.77	1	79.77	0.0942	0.7641	
D-Rotation speed	7866.88	1	7866.88	9.29	0.0101	
AB	1193.01	1	1193.01	1.41	0.2581	
AC	6707.61	1	6707.61	7.92	0.0156	
AD	217.56	1	217.56	0.2570	0.6214	
BC	16283.04	1	16283.04	19.24	0.0009	
BD	1954.52	1	1954.52	2.31	0.1545	
CD	23490.16	1	23490.16	27.75	0.0002	
A <sup>2</sup>	19783.57	1	19783.57	23.37	0.0004	
B <sup>2</sup>	12986.95	1	12986.95	15.34	0.0020	

Source	Sum of squares	df	Mean square	F-value	p-value	
C <sup>2</sup>	881.68	1	881.68	1.04	0.3276	
D <sup>2</sup>	12600.36	1	12600.36	14.89	0.0023	
Residual	10157.78	12	846.48			
Lack of Fit	9256.92	10	925.69	2.06	0.3715	Not significant
Pure Error	900.86	2	450.43			
<b>Cor Total</b>	1.152E+05	26				

Among the primary factors, Ball Diameter (B) and Rotation Speed (D) emerge as significant contributors to particle size reduction, as indicated by their respective p-values of 0.0183 and 0.0101. In contrast, Time (A) and BW/MW Ratio (C) show no statistically meaningful individual effect ( $p > 0.75$ ), suggesting limited influence when considered in isolation.

Several two-factor interactions demonstrate significance, notably AC (time  $\times$  BW/MW Ratio,  $p = 0.0156$ ), BC (Ball Diameter  $\times$  BW/MW Ratio,  $p = 0.0009$ ), and CD (B/WM Ratio  $\times$  Rotation Speed,  $p = 0.0002$ ). These interactions highlight the complex, interdependent nature of the milling process. Conversely, interactions such as AB, AD, and BD do not show statistical relevance.

Quadratic terms for Time (A<sup>2</sup>), Ball Diameter (B<sup>2</sup>), and Rotation Speed (D<sup>2</sup>) are all highly significant ( $p < 0.005$ ), underscoring the presence of non-linear behaviour in the system. However, the quadratic term for BW/MW Ratio (C<sup>2</sup>) is not significant ( $p = 0.3276$ ), indicating a limited non-linear effect.

Taken together, the results affirm the suitability of a quadratic regression model for capturing the multidimensional, non-linear dynamics governing cathodic material size reduction during milling.

### 3.3. Surface plots and perturbation analysis (pre-leaching)

Figure 4a compares the predicted and actual values, confirming the model's accuracy. The perturbation curve in Figure 4b highlights ball diameter and BW/MW ratio as the most influential parameters. Surface plots in Figure 5 illustrate optimal parameter ranges for achieving the greatest nanoscale conversion.

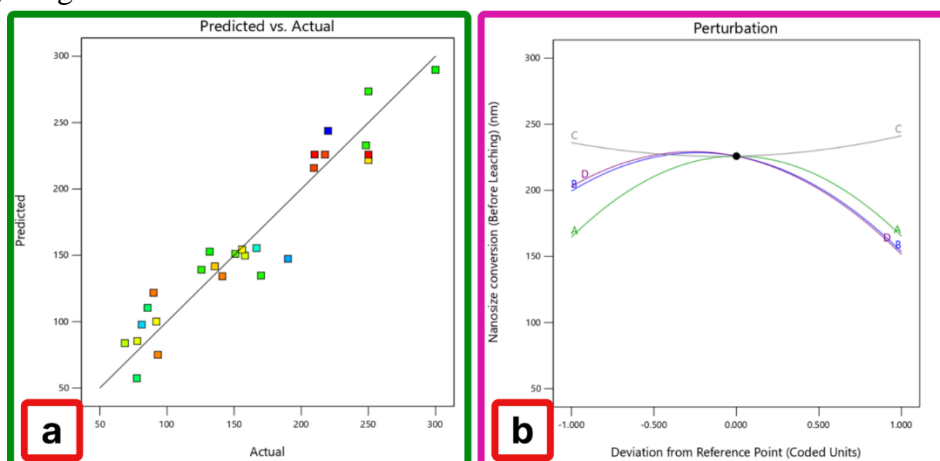


**Figure 4.** (a) Graph of predicted value Vs actual value for cathodic material size reduction before leaching; (b) perturbation curve of cathodic material for nano conversion before leaching.

Figure 4 (a) presents a graph contrasting the expected and actual values for the decrease in cathodic material size before leaching, therefore offering a graphic evaluation of the predictive power of the model. Based on nanosized conversion after leaching, the data points are color-coded within the range of 37.84 nm to 190 nm, providing further understanding of

how post-leaching nanosized results correlate with pre-leaching forecasts. With little difference between predicted and actual values, most data points' close grouping around the 45-degree reference line indicates strong model performance. This congruence implies that the model captures nanosized conversion behaviour before leaching with reasonable precision.

Particularly in the central and larger-size domains, the distribution of data points across the full range of actual values demonstrates the model's resilience in forecasting under different conditions. Though small deviations exist, the absence of any obvious bias pattern suggests that the model residuals are randomly distributed, thereby supporting the accuracy of the forecasts.

Moreover, the homogeneous distribution of colour along the reference line indicates that nanosized conversion following leaching does not significantly interfere with or skew the model's predictive capability prior to leaching. This consistency confirms earlier statistical results, including high  $R^2$  values and minimal residual errors from ANOVA and F-value analyses, thereby verifying the generalizability and accuracy of the model across several experimental settings.

Figure 4(b) presents the perturbation plot, which delineates the individual influence of four critical process parameters, Ball Diameter (A), BW/MW ratio (B), Rotational Speed (C), and Time (D), on the nanosized conversion of the cathodic material prior to leaching. This graphical representation is instrumental for assessing the sensitivity of the response variable to variations in each factor, while holding all other variables constant at their respective reference values.

The perturbation curves reveal that Ball Diameter (A), BW/MW ratio (B), and Time (D) exhibit pronounced curvature, indicative of a non-linear relationship with nanosized conversion. As these variables increase from their lower bounds toward the central reference point, the efficiency of size reduction improves. However, surpassing optimal thresholds leads to a decline in conversion performance. This parabolic trend suggests the existence of optimal process windows, beyond which inefficiencies such as particle agglomeration, excessive energy input, or heat-induced effects may counteract the benefits of continued size reduction.

Conversely, the curve for Rotational Speed (C) is notably flatter, with minimal deviation from the baseline, suggesting that within the investigated range, changes in rotational speed exert a comparatively modest effect on the response. While this parameter may contribute to the overall grinding dynamics, its isolated influence appears limited when other variables are held constant.

The perturbation analysis underscores the dominant roles of Ball Diameter, BW/MW ratio, and Time in governing the nanosized conversion process. Their optimization is essential for maximizing efficiency before leaching. Rotational Speed, while not negligible, appears to play a secondary or supportive role within the studied operational window.

The 3D surface plots in Figure 5 elucidate the interactive effects of various process parameters on the nanosized conversion of the cathodic material prior to leaching. Each subplot shows a two-factor interaction, highlighting how parameter combinations influence the degree of size reduction.

Plot (a) represents the interaction between Ball Diameter and Time, revealing a curved response surface with a well-defined peak. This indicates the presence of an optimal region where the synergy between ball size and milling duration maximizes nanosized conversion. Both insufficient and excessive milling times, when coupled with either very small or large

ball diameters, tend to reduce the conversion efficiency, likely due to phenomena such as under-grinding or excessive agglomeration from over-grinding.

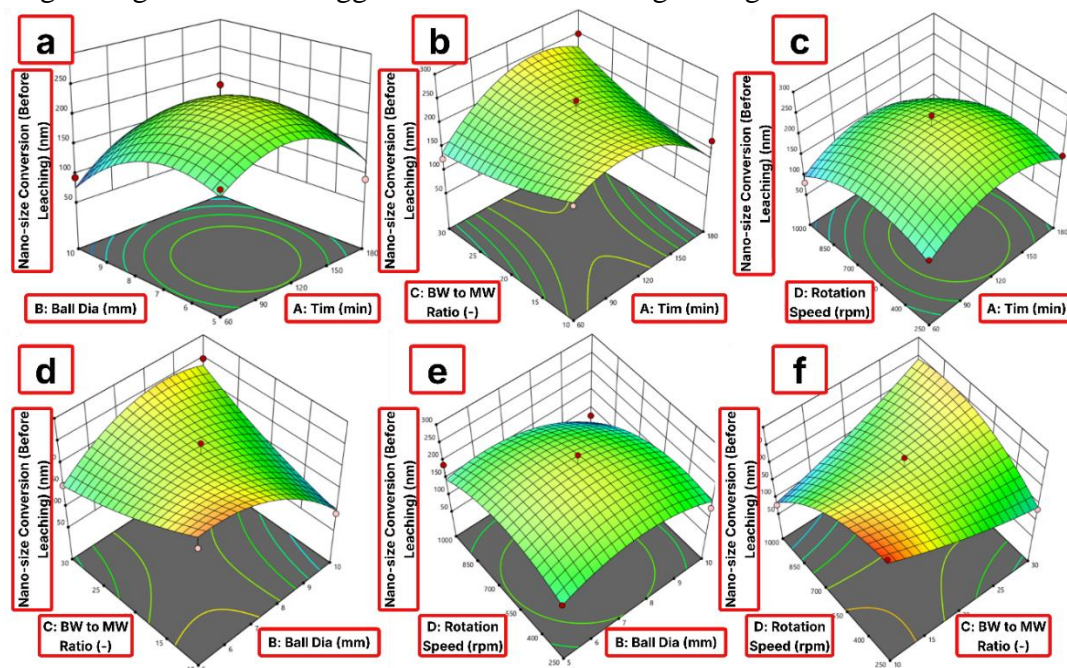


**Figure 5.** 3D Surface interactions plots before leaching, (a) ball Dia Vs time; (b) BW/MW ratio Vs time; (c) rotational speed vs time; (d) BW/MW ratio vs ball Dia; (e) Rotational speed vs ball Dia; (f) Rotational speed Vs BW/MW ratio.

Plot (b) displays the effect of the BW/MW ratio and Time, exhibiting a pronounced curvature. The nanosized conversion increases with milling time, particularly at moderate BW/MW ratios. Extremely low or high ratios, however, lead to reduced efficiency, likely due to either inadequate impact force or excessive cushioning between particles, limiting the effectiveness of size reduction.

Plot (c) shows the interaction between Rotational Speed and Time, where a dome-shaped surface suggests that optimal grinding occurs at intermediate values of both parameters. High rotational speeds or prolonged durations may result in reduced performance, potentially due to the onset of thermal effects or particle re-agglomeration, which counteract the desired fragmentation.

Plot (d) investigates the relationship between the BW/MW ratio and Ball Diameter. The surface indicates improved size reduction with increasing ball diameter, particularly at moderate BW/MW ratios. However, further increases beyond certain thresholds in either parameter do not yield proportional benefits and may even hinder nanosized conversion due to suboptimal impact dynamics.

Plot (e) highlights the interactive effect of Rotational Speed and Ball Diameter, revealing a distinct region where medium-to-high speeds combined with mid-sized balls produce the highest nanosize conversion. Deviation from these optimal values compromises grinding efficiency, possibly due to altered energy-transfer mechanisms and reduced particle fracture rates.

Plot (f) examines the relationship between Rotational Speed and the BW/MW ratio. The conversion trend shows a consistent increase with both parameters, especially under high rotational speeds and moderate-to-high BW/MW ratios. This combination appears to provide sufficient kinetic energy and particle motion to facilitate effective size reduction.

### 3.4. Statistical model fit for post-leaching

As shown in Table 5, ANOVA identified rotation speed ( $p < 0.0001$ ) and its squared term as the most critical parameters post-leaching. Other significant interactions include AB, AD, and CD. The model fit was strong, with a non-significant lack of fit ( $p = 0.2138$ ) and low residual error.

**Table 5.** F and P values for cathodic material reduction after leaching.

Source	Sum of squares	df	Mean square	F-value	p-value	
Model	40558.62	14	2897.04	24.99	< 0.0001	Significant
A-Time	134.13	1	134.13	1.16	0.3032	
B-Ball Dia	103.02	1	103.02	0.8886	0.3644	
C-BW/MW Ratio	1046.45	1	1046.45	9.03	0.0110	
D-Rotation speed	7229.48	1	7229.48	62.36	< 0.0001	
AB	6475.42	1	6475.42	55.86	< 0.0001	
AC	2281.97	1	2281.97	19.68	0.0008	
AD	2382.42	1	2382.42	20.55	0.0007	
BC	367.87	1	367.87	3.17	0.1002	
BD	1437.17	1	1437.17	12.40	0.0042	
CD	6119.93	1	6119.93	52.79	< 0.0001	
A <sup>2</sup>	1373.31	1	1373.31	11.85	0.0049	
B <sup>2</sup>	6961.69	1	6961.69	60.05	< 0.0001	
C <sup>2</sup>	3424.39	1	3424.39	29.54	0.0002	
D <sup>2</sup>	9754.60	1	9754.60	84.14	< 0.0001	
Residual	1391.19	12	115.93			
Lack of Fit	1325.83	10	132.58	4.06	0.2138	not significant
Pure Error	65.36	2	32.68			
Cor Total	41949.81	26				

Regarding interactions, numerous two-factor combinations are highly significant, as illustrated in Table 5. The interactions AB (Time × Ball Diameter), AC (Time × BW/MW Ratio), AD (Time × Rotation Speed), BD (Ball Diameter × Rotation Speed), and CD (BW/MW ratio × Rotation Speed) exhibit very low p-values ( $< 0.005$ ), indicating significant interactive effects among these parameter pairs on the final particle size. This highlights the significance of examining not only individual elements but also their collective impacts during the optimization process.

Upon examining the quadratic terms, it is evident that all four squared terms, A<sup>2</sup>, B<sup>2</sup>, C<sup>2</sup>, and D<sup>2</sup>, demonstrate statistical significance, with D<sup>2</sup> (Rotation Speed squared) emerging as the most impactful ( $F = 84.14$ ,  $p < 0.0001$ ). This indicates a significant curvature in the response surface, especially concerning rotation speed. The residual sum of squares for the model is relatively low (1391.19), and the lack-of-fit test is not significant ( $p = 0.2138$ ). This suggests a strong fit of the quadratic model to the data, with the residual variability mainly attributable to pure error rather than to any inadequacy of the model itself.

The findings indicate that a quadratic model effectively captures the impact of the process parameters, with rotation speed and its interactions being the most significant factors in reducing cathodic material size following leaching.

### 3.5. Surface plots and perturbation analysis (pre-leaching)

Figure 6a shows close alignment between predicted and experimental values. The perturbation plot in Figure 6b emphasizes the importance of rotation speed and BW/MW ratio. 3D surface plots in Figure 7 reveal synergistic effects among variables, particularly between rotation speed and the BW/MW ratio.

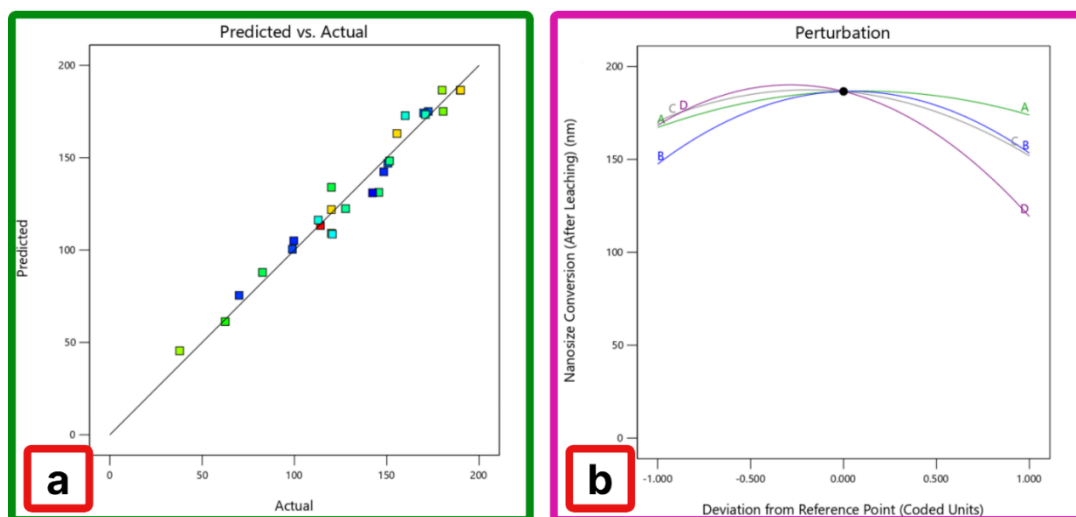


**Figure 6.** (a) Graph of predicted value Vs actual value for cathodic material size reduction after leaching; (b) Perturbation curve of cathodic material for nano conversion after leaching

Figure 6(a) illustrates a comparison of predicted and actual values for the reduction in cathodic material size following leaching, providing a visual assessment of the model's predictive precision. The data points are coloured by material size before leaching, spanning 68.6 nm to 300 nm. This provides further insight into the potential relationship between initial particle size and prediction accuracy. The tight clustering of points near the 45-degree reference line suggests that the model performs well, with little variation between predicted and experimental values.

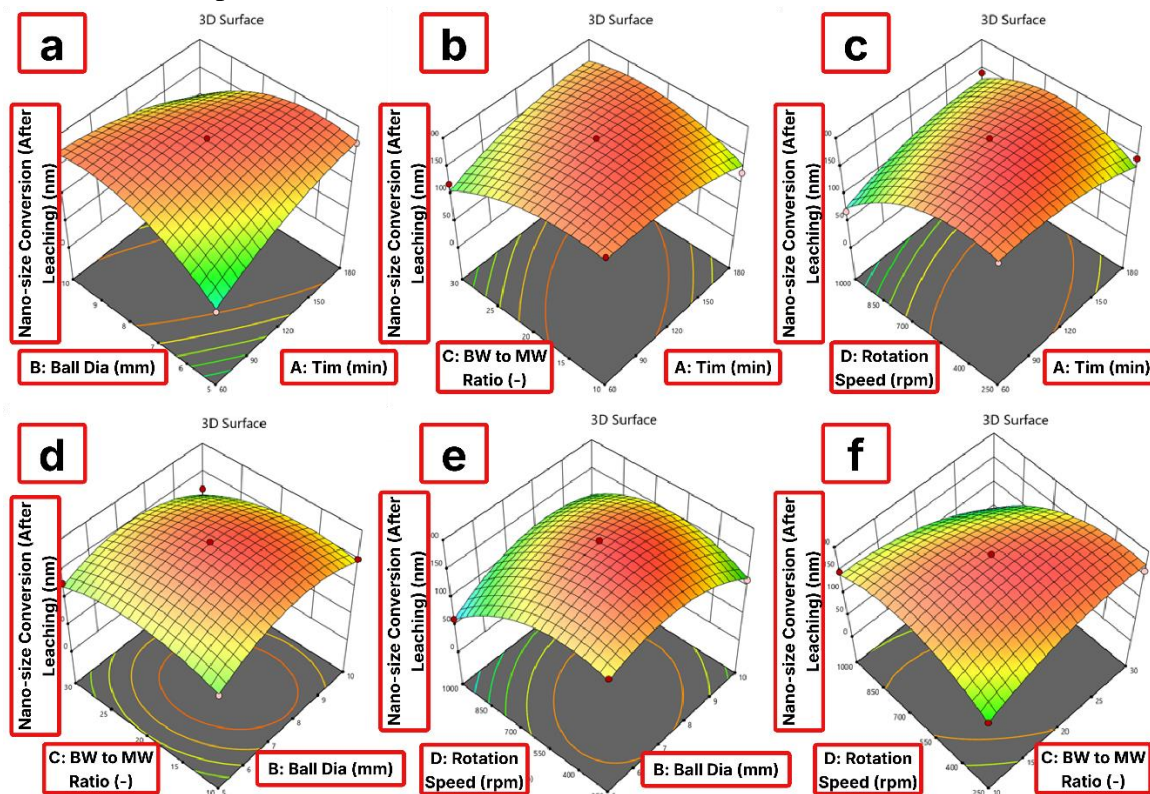
The uniformity in data distribution across the value spectrum, particularly in the central and upper segments of the actual size range, highlights the model's strength and reliability in forecasting post-learning nanosized results. Minor deviations are noted, and there are no discernible patterns of systematic error, suggesting that the model is free from substantial bias. This alignment corroborates the statistical findings of elevated  $R^2$  and minimal residual error observed in prior ANOVA and F-value analyses. Moreover, the uniform distribution of colour along the line indicates that the initial nanosized particles do not significantly degrade the model's predictive ability, thereby strengthening its applicability across various input scenarios.

Figure 6 (b) presents the perturbation curve for the nanosized conversion of cathodic material following leaching, offering a detailed examination of how the response variable is influenced by specific process parameters: A (Time), B (Ball Diameter), C (BW/MW Ratio), and D (Rotation Speed). The curve assesses the impact of each variable while holding the others at their reference levels (A = 120 min, B = 7.5 mm, C = 20, D = 625 rpm), thereby providing a comparative analysis of each factor's influence.

Among the variables, factor D (Rotation Speed), illustrated by the purple curve, shows the most pronounced curvature, suggesting that nanosized conversion is particularly responsive to rotation speed variations. A minor deviation from the reference point results in a significant reduction in nanosized conversion, underscoring the critical role of high-energy milling dynamics. In a similar vein, factor C (BW/MW Ratio) shows a significant effect, albeit less pronounced than D, underscoring the critical role of optimizing mass ratios during milling. Factor B (Ball Diameter) exhibits a moderately curved response, indicating it has a notable yet relatively lesser impact. In the meantime, factor A (Time), depicted in green, seems to exhibit

the most consistent or minimal impact within the examined range, characterized by a relatively flat curve.

The perturbation plot clearly indicates that rotation speed (D) and the BW/MW ratio (C) play essential roles in attaining successful nanosized conversion after leaching. Adjusting these parameters can greatly enhance the leaching efficiency and the quality of the nanoscale cathodic material produced.



**Figure 7.** 3D Surface plots interactions after leaching, (a) Ball Dia Vs time; (b) BW/MW ratio vs time; (c) rotational speed vs time; (d) BW/MW ratio vs ball Dia; (e) Rotational speed vs ball Dia; (f) rotational speed vs BW/MW ratio

Figure 7 displays six 3D surface plots illustrating the interactions among different ball-milling parameters on the nanosized conversion of cathodic material following leaching. These plots provide a detailed visual representation of the interplay between pairs of variables and their collective impact on the response, specifically regarding post-leaching particle-size reduction.

In plot (a), the relationship between ball diameter and time exhibits a distinct upward curvature, indicating that as time increases, there is a notable enhancement in nanosized conversion, particularly at moderate ball diameters. Nonetheless, it appears that excessively large ball diameters may lead to a slight decrease in conversion, suggesting an optimal range for maximizing energy transfer during milling. Plot (b) examines the influence of time and the ratio of BW/MW. Nanosized conversion is enhanced with increased BW/MW ratios and extended milling durations, suggesting that longer milling, when paired with an adequate material load, facilitates efficient particle fragmentation.

The plot (c) illustrates the relationship between rotational speed and time, showing that an increase in rotational speed markedly improves nanosized conversion, especially during extended milling. The red area at the top of the plot signifies the most effective combinations of increased rotation speed and adequate milling duration. In plot (d), the interplay between the BW/MW ratio and ball diameter demonstrates a synergistic effect, indicating that moderate

ball sizes combined with higher material loading ratios result in enhanced conversion rates. This highlights the significance of mechanical collision frequency and the balance of mass transfer.

The plot illustrates the relationship between rotation speed and ball diameter, showing that rotation speed is the primary factor in particle size reduction, while ball diameter becomes less significant after reaching a threshold. Finally, plot (f) assesses the impact of rotation speed and the BW/MW ratio, revealing that elevated rotation speeds, when paired with ideal material loading, yield the highest conversion to nanosized particles following leaching.

In summary, the surface plots indicate that rotational speed and the BW/MW ratio are the key parameters, frequently producing a more pronounced synergistic effect when paired with appropriate time and ball diameter configurations. Meticulous optimization of these parameter combinations is crucial for attaining the targeted nano-level reduction of cathodic materials.

### 3.6. Optimal parameter identification.

Table 6 presents the optimal conditions: 60 minutes milling time, 5 mm ball diameter, 30:1 BW/MW ratio, and 650 rpm. These parameters yielded an experimental post-leaching particle size of 117.5 nm, with prediction errors below 5%, confirming the robustness of the model and optimization strategy.

**Table 6.** Optimal solutions for nanosized conversion

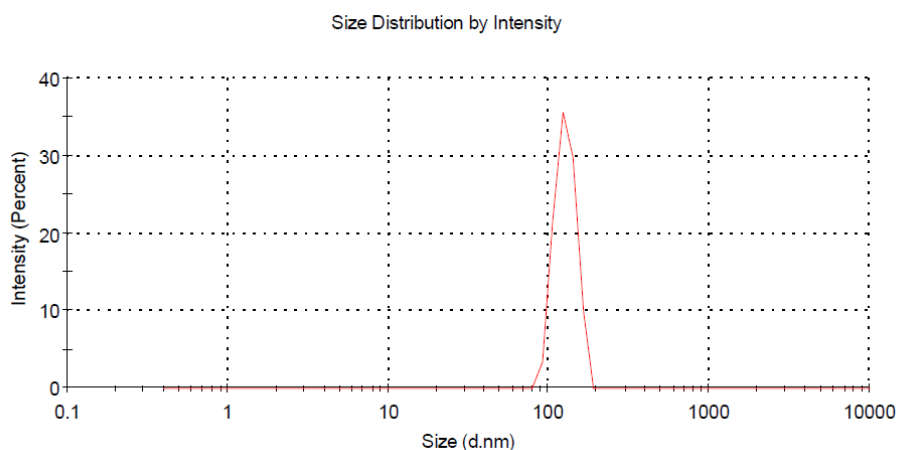
S.No.	Time (min)	Ball diameter (mm)	BW/MW Ratio	RPM	Predicted Material Size Before Leaching	Experimental Material Size BL	Error %	Predicted Material Size After Leaching	Experimental Material Size AL	Error %
1	60	5	30	650	131.8	135.3	2.65554	112.9	117.5	4.0744

Table 6 outlines the optimal values for the nanosized conversion of LiCoO<sub>2</sub> cathodic material. Four essential variables—Time, ball size, BW/MW ratio, and rotational speed—were optimized in relation to one another. The optimal parameters—60 minutes of milling, a ball diameter of 5 mm, a ratio of 30:1, and a speed of 650 RPM—yielded a predicted pre-leaching particle size of 131.8 nm, which closely aligns with the experimentally measured value of 135.3 nm, resulting in a minimal error of 2.66%. The model predicted a size of 112.9 nm, while the experimental measurement was 117.5 nm, resulting in a 4.07% error. Following the leaching process, the particle size decreased even more. The strong alignment between expected and observed values validates the robustness of the optimization model. It highlights the efficacy of the process parameters in achieving notable nanoscale reduction of the cathodic material.

### 3.7. Material characterization results

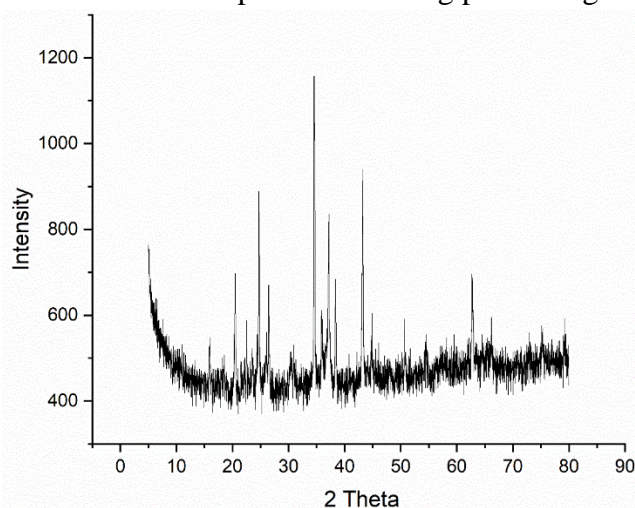
To confirm the nanoscale nature and structural integrity of the recovered cathodic material, particle size analysis (PSA) and X-ray diffraction (XRD) were performed on selected optimal samples.

Figure 8 presents the particle size distribution curve obtained from PSA for the sample treated under optimal conditions (Run 1: 60 min, 5 mm, 30:1, 650 rpm). The distribution peak centered at 117.5 nm confirms successful reduction to the nanoscale.



**Figure 8.** Particle size distribution of the sample as measured by Dynamic Light Scattering (DLS), showing a narrow peak centered around ~100 nm. The sharp, monomodal distribution indicates a uniform population of nanosized particles with minimal aggregation.

Figure 9 shows the XRD pattern of the same sample. The dominant peaks observed at  $2\theta$  values of  $\sim 18.7^\circ$ ,  $37.3^\circ$ ,  $44.7^\circ$ , and  $65.1^\circ$  are characteristic of the layered  $\text{LiCoO}_2$  phase, as indexed to the JCPDS Card No. 50-0653. The presence of sharp, well-defined peaks indicates that the material's crystalline nature was preserved during processing.



**Figure 9.** X-ray diffraction (XRD) pattern of the sample showing characteristic peaks in the  $2\theta$  range of  $5^\circ$  to  $80^\circ$ . The sharp and well-defined peaks indicate a crystalline structure, while the broad background suggests the presence of some amorphous content or nanosized crystallites.

Additionally, elemental composition was verified using inductively coupled plasma optical emission spectroscopy (ICP-OES), confirming lithium and cobalt content within the expected range.

These analyses validate the nanoscale dimension and phase stability of the recovered cathodic material, confirming the effectiveness of the sequential processing and milling strategy.

### 3.8. Sustainability considerations

The study used a sequence of experiments called DR, PT, and HT that were meant to follow the principles of a circular economy by minimizing waste, extending the life of products, and reducing the need for new raw materials.

Energy Use: PT (800°C for 8 hours) uses the most energy of all the phases. This procedure is performed only once, but it removes carbon and restores crystallinity, making it easier to recover materials later. The HT stage employed 1.25 M citric acid and 1% H<sub>2</sub>O<sub>2</sub> as reagents and heated them to 90°C. This made it safer and better for the environment than using powerful acids.

Minimizing Waste: Ball milling is a mechanical method for reducing particle size that consumes a lot of energy but offers excellent leaching efficiency, resulting in less reagent consumption in the HT phase and less chemical waste.

Environmental Trade-Off: The method avoids the use of highly toxic solvents and the complex separation processes common in commercial recycling lines. Instead, it uses low-toxicity and reusable reagents. This makes the procedure more eco-friendly.

Overall, even if numerical metrics (such as CO<sub>2</sub> emissions or energy per gram of product) were not assessed, the process was built with a low-footprint, lab-scale green processing mindset. This provides a solid foundation for future studies on how to measure and scale up sustainability.

#### 4. Conclusion

This study outlines a detailed, methodical framework to enhance the extraction and nanoscale size reduction of cathodic LiCoO<sub>2</sub> from spent lithium-ion batteries. It employs a sequential recycling strategy that combines direct recycling, pyrometallurgical processing, and hydrometallurgical leaching. The innovative integration of these methods, coupled with a statistically rigorous parametric optimization through RSM, facilitated the identification of key ball milling parameters, ball diameter, BW/MW ratio, rotation speed, and milling time, that dictate the transition of cathodic material from micron to nanoscale.

The results indicate that, prior to leaching, the ball diameter and rotation speed are the key factors, whereas after leaching, rotation speed and its interactions with other variables become the primary influences. The quadratic regression models developed for the pre- and post-leaching stages demonstrated strong predictive accuracy, as evidenced by high R<sup>2</sup> values, minimal residual errors, and a close alignment between predicted and actual particle sizes. The analysis of perturbation and 3D surface interaction plots highlighted the complex, interdependent nature of the process variables, facilitating the accurate determination of optimal parameter combinations.

The optimal solution involved 60 minutes of milling using 5 mm balls, a ball-to-material ratio of 30:1, and a speed of 650 rpm. This approach resulted in nearly perfect conversion to nanosized particles, with experimental errors remaining below 5% for both pre- and post-leaching particle sizes. The findings validate the model's reliability and demonstrate the proposed methodology's success in achieving substantial particle size reduction while maintaining structural integrity and performance.

This experimental study presents a validated and scalable approach for the sustainable recovery of resources from lithium-ion battery waste. The integration of advanced recycling techniques with smart process optimization not only improves material recovery efficiency but also fosters the development of sustainable circular-economy solutions within the energy storage industry.

## Author Contributions

Conceptualization, V.K.S. and V.P.S.; methodology, V.P.S. and S.J.; software, V.K.S.; validation, S.J.; formal analysis, V.K.S., V.P.S., and S.J.; investigation, V.K.S.; resources, V.K.S. and S.J.; data curation, V.K.S.; writing—original draft preparation, V.K.S.; writing—review and editing, V.P.S. and S.J.; visualization, V.K.S. and S.J.; supervision, V.P.S. and S.J.; project administration, V.P.S.; funding acquisition, S.J. All authors have read and agreed to the published version of the manuscript.

## Informed Consent Statement

Not applicable.

## Data Availability Statement

Data supporting the findings of this study are available upon reasonable request from the corresponding author.

## Funding

This work received financial support from the 'Starting Research grant, Science and Engineering Research Board, Department of Science and Technology, India, under grant no." SRG/2023/001949 "and supported by UPES R&D under the UPES-SEED grant program, under grant no. "UPES/R&D-SoAE/08042024/5).

## Acknowledgements

This work acknowledges the resources provided by the Science and Engineering Research Board, Department of Science and Technology, India; the Department of Mechanical Engineering; and the R&D Department of UPES, Dehradun, India.

## Conflicts of Interest

The authors declare no conflict of interest.

## Abbreviations

Abbreviation	Definition
DR	Direct Recycling
PR	Pyrometallurgical Recycling
HR	Hydrometallurgical Recycling
PT	Pyrometallurgical Treatment
HT	Hydrometallurgical Treatment
XRD	X-Ray Diffraction
PSA	Particle Size Analysis
FESEM	Field Emission Scanning Electron Microscopy
ICP-OES	Inductively Coupled Plasma Optical Emission Spectrometry
DoE	Design of Experiments
RSM	Response Surface Methodology
BBD	Box–Behnken design
ANOVA	Analysis of Variance

Abbreviation	Definition
EU	European Union
Nm	Nanometre
µm	Micrometre
Rpm	Revolutions per minute
EPR	Extended Producer Responsibility
Mn	Manganese
Mg	Magnesium
LiCoO <sub>2</sub>	Lithium Cobalt Oxide
LIBs	Lithium-Ion Batteries
H <sub>2</sub> SO <sub>4</sub>	Sulfuric Acid
CO <sub>2</sub>	Carbon Dioxide
EVs	Electric Vehicles
Ni-Co	Nickel-Cobalt Alloys
H <sub>2</sub> O <sub>2</sub>	Hydrogen Peroxide
HNO <sub>3</sub>	Nitric Acid
BW/MW	Ball Weight to Material Weight
F-value	Fisher Value
p-value	Probability Value
R <sup>2</sup> values	Coefficient of Determination
EoL	End-of-Life
Li	Lithium
Co	Cobalt
O	Oxygen
Cu	Copper
Mol	Mole
S/L	Solid–Liquid Ratio
kW	Kilowatt

## References

- Roy, J.J.; Rarotra, S.; Krikstolaityte, V.; Zhuoran, K.W.; Cindy, Y.D.I.; Tan, X.Y.; Carboni, M.; Meyer, D.; Yan, Q.; Srinivasan, M. Green recycling methods to treat lithium-ion batteries E-waste: a circular approach to sustainability. *Advanced Materials* **2022**, *34*, 2103346, <https://doi.org/10.1002/adma.202103346>.
- Jin, S.; Mu, D.; Lu, Z.; Li, R.; Liu, Z.; Wang, Y.; Tian, S.; Dai, C. A comprehensive review on the recycling of spent lithium-ion batteries: Urgent status and technology advances. *Journal of Cleaner Production* **2022**, *340*, 130535, <https://doi.org/10.1016/j.jclepro.2022.130535>.
- Sharma, N.; Kalbar, P.P.; Salman, M. Global review of circular economy and life cycle thinking in building Demolition Waste Management: A way ahead for India. *Building and Environment* **2022**, *222*, 109413, <https://doi.org/10.1016/j.buildenv.2022.109413>.
- Lebrouhi, B.E.; Baghi, S.; Lamrani, B.; Schall, E.; Kousksou, T. Critical materials for electrical energy storage: Li-ion batteries. *Journal of Energy Storage* **2022**, *55*, 105471, <https://doi.org/10.1016/j.est.2022.105471>.
- Golmohammadzadeh, R.; Faraji, F.; Jong, B.; Pozo-Gonzalo, C.; Banerjee, P.C. Current challenges and future opportunities toward recycling of spent lithium-ion batteries. *Renewable and Sustainable Energy Reviews* **2022**, *159*, 112202, <https://doi.org/10.1016/j.rser.2022.112202>.
- Olabi, A.G.; Abbas, Q.; Shinde, P.A.; Abdelkareem, M.A. Rechargeable batteries: Technological advancement, challenges, current and emerging applications. *Energy* **2023**, *266*, 126408, <http://dx.doi.org/10.1016/j.energy.2022.126408>.
- Kumar, A.; Gaur, D.; Liu, Y.; Sharma, D. Sustainable waste electrical and electronic equipment management guide in emerging economies context: A structural model approach. *Journal of Cleaner Production* **2022**, *336*, 130391, <https://doi.org/10.1016/j.jclepro.2022.130391>.

8. Kurniawan, T.A.; Maiurova, A.; Kustikova, M.; Bykovskaia, E.; Othman, M.H.D.; Goh, H.H. Accelerating sustainability transition in St. Petersburg (Russia) through digitalization-based circular economy in waste recycling industry: A strategy to promote carbon neutrality in era of Industry 4.0. *Journal of cleaner production* **2022**, *363*, 132452, <https://doi.org/10.1016/j.jclepro.2022.132452>.
9. Zhang, X.; Khaskheli, M.B.; Shen, C.; Jafri, M.A.H.; Shamsi, I.H. A comparative study of economic activity and sustainable development in China and Three South Asian Countries. *Discover Sustainability* **2025**, *6*, 170, <http://dx.doi.org/10.1007/s43621-025-00885-8>.
10. Compagnoni, M.; Grazi, M.; Pieri, F.; Tomasi, C. Extended producer responsibility and trade flows in waste: The case of batteries. *Environmental and Resource Economics* **2025**, *88*, 43-76, <https://doi.org/10.1007/s10640-024-00907-5>.
11. Jiang, C.; Zhang, Y. Does Extended Producer Responsibility System Promote Green Technological Innovation in China's Power Battery Enterprises? *Sustainability* **2023**, *15*, 12318, <https://doi.org/10.3390/su151612318>.
12. Dar, A.A.; Chen, Z.; Zhang, G.; Hu, J.; Zaghbi, K.; Deng, S.; Wang, X.; Haghghat, F.; Mulligan, C.N.; An, C. Sustainable extraction of critical minerals from waste batteries: A green solvent approach in resource recovery. *Batteries* **2025**, *11*, 51, <https://doi.org/10.3390/batteries11020051>.
13. Wang, Z.; Huang, G.; Chen, Z.; An, C. Accidents involving lithium-ion batteries in non-application stages: incident characteristics, environmental impacts, and response strategies. *BMC chemistry* **2025**, *19*, 94, <https://doi.org/10.1186/s13065-025-01445-x>.
14. Khan, S.R.; Khan, M.M.; Srivastava, K.; Jin, H.; Plante, L.; Lee, J.J.; Barstow, B.; Reed, D.W.; Alvarez, R.S. Sustainable recovery of critical metals from spent lithium-ion batteries through gluconic acid-based bioleaching: Techno-economic analysis, life cycle assessment and process optimization. *Chemical Engineering Journal* **2025**, *516*, 163714, <https://doi.org/10.1016/j.cej.2025.163714>.
15. Santos, A.L.; Alves, W.; Ferreira, P. Challenges faced by lithium-ion batteries in effective waste management. *Sustainability* **2025**, *17*, 2893, <https://doi.org/10.3390/su17072893>.
16. Liang, X.; Tang, J.; Li, L.; Wu, Y.; Sun, Y. A review of metallurgical processes and purification techniques for recovering Mo, V, Ni, Co, Al from spent catalysts. *Journal of Cleaner Production* **2022**, *376*, 134108, <https://doi.org/10.1016/j.jclepro.2022.134108>.
17. Yang, Y.; Wang, R.; Shen, Z.; Yu, Q.; Xiong, R.; Shen, W. Towards a safer lithium-ion batteries: A critical review on cause, characteristics, warning and disposal strategy for thermal runaway. *Advances in Applied Energy* **2023**, *11*, 100146, <https://doi.org/10.1016/j.adapen.2023.100146>.
18. Qing, J.; Wu, X.; Zeng, L.; Guan, W.; Cao, Z.; Li, Q.; Wang, M.; Zhang, G.; Wu, S. Novel approach to recycling of valuable metals from spent lithium-ion batteries using hydrometallurgy, focused on preferential extraction of lithium. *Journal of Cleaner Production* **2023**, *431*, 139645, <https://doi.org/10.1016/j.jclepro.2023.139645>.
19. Wiszniewski, L.; Marschall, I.; Hochsteiner, T.; Hoad, T.M.; Döschek-Held, K.; Raupenstrauch, H. Evaluating refractory material performance in pyrometallurgical recycling of lithium-ion batteries under a reducing atmosphere. *Ceramics International* **2024**, *50*, 43683-43698, <https://doi.org/10.1016/j.ceramint.2024.08.220>.
20. Li, X.; Ma, B.; Wang, C.; Chen, Y. Sustainable recovery and recycling of scrap copper and alloy resources: A review. *Sustainable Materials and Technologies* **2024**, *41*, e01026, <https://doi.org/10.1016/j.susmat.2024.e01026>.
21. Shin, Y.; Kim, S.; Park, S.; Lee, J.; Bae, J.; Kim, D.; Joo, H.; Ban, S.; Lee, H.; Kim, Y. A comprehensive review on the recovery of cathode active materials via direct recycling from spent Li-ion batteries. *Renewable and Sustainable Energy Reviews* **2023**, *187*, 113693, <https://doi.org/10.1016/j.rser.2023.113693>.
22. Binnemans, K.; Jones, P.T. The twelve principles of circular hydrometallurgy. *Journal of Sustainable Metallurgy* **2023**, *9*, 1-25, <https://link.springer.com/article/10.1007/s40831-022-00636-3>.
23. Vieceli, N.; Casasola, R.; Lombardo, G.; Ebin, B.; Petranikova, M. Hydrometallurgical recycling of EV lithium-ion batteries: Effects of incineration on the leaching efficiency of metals using sulfuric acid. *Waste Management* **2021**, *125*, 192-203, <https://doi.org/10.1016/j.wasman.2021.02.039>.
24. Wei, L.K.; Abd Rahim, S.Z.; Al Bakri Abdullah, M.M.; Yin, A.T.M.; Ghazali, M.F.; Omar, M.F.; Nemeş, O.; Sandu, A.V.; Vizureanu, P.; Abdellah, A.E.-h. Producing metal powder from machining chips using ball milling process: A review. *Materials* **2023**, *16*, 4635, <https://doi.org/10.3390/ma16134635>.

25. Ashraf, W.; Khan, A.; Bansal, S.; Khanuja, M. Mechanical ball milling: A sustainable route to induce structural transformations in tungsten disulfide for its photocatalytic applications. *Physica E: Low-dimensional Systems and Nanostructures* **2022**, *140*, 115152, <https://doi.org/10.1016/j.physe.2022.115152>.
26. Wei, M.; Wang, B.; Chen, M.; Lyu, H.; Lee, X.; Wang, S.; Yu, Z.; Zhang, X. Recent advances in the treatment of contaminated soils by ball milling technology: Classification, mechanisms, and applications. *Journal of Cleaner Production* **2022**, *340*, 130821, <https://doi.org/10.1016/j.jclepro.2022.130821>.
27. Joy, J.; Krishnamoorthy, A.; Tanna, A.; Kamathe, V.; Nagar, R.; Srinivasan, S. Recent developments on the synthesis of nanocomposite materials via ball milling approach for energy storage applications. *Applied Sciences* **2022**, *12*, 9312, <https://doi.org/10.3390/app12189312>.
28. Agnihotri, M.; Chamola, R.; Bhan, U.; Jain, S. Analyzing the performance of synthesized nano-catalysts for transesterification of waste cooking oil as environment friendly drilling fluid. *Environmental Research* **2024**, *244*, 117948, <https://doi.org/10.1016/j.envres.2023.117948>.

### **Publisher's Note & Disclaimer**

The statements, opinions, and data presented in this publication are solely those of the individual author(s) and contributor(s) and do not necessarily reflect the views of the publisher and/or the editor(s). The publisher and/or the editor(s) disclaim any responsibility for the accuracy, completeness, or reliability of the content. Neither the publisher nor the editor(s) assume any legal liability for any errors, omissions, or consequences arising from the use of the information presented in this publication. Furthermore, the publisher and/or the editor(s) disclaim any liability for any injury, damage, or loss to persons or property that may result from the use of any ideas, methods, instructions, or products mentioned in the content. Readers are encouraged to independently verify any information before relying on it, and the publisher assumes no responsibility for any consequences arising from the use of materials contained in this publication.